Shaking-table tests of flat-bottom circular silos containing grain-like material

Stefano Silvestri[1], Salvador Ivorra[2], Laura Di Chiacchio[1], Tomaso Trombetti[1], Dora Foti[3], Giada Gasparini[1], Luca Pieraccini[1], Matt Dietz[4], Colin Taylor[4]

[1] *Department DICAM, University of Bologna, Italy*
[2] *Department of Civil Engineering. University of Alicante, Spain*
[3] *Department DICA, Technical University of Bari, Italy*
[4] *Department of Civil Engineering. University of Bristol, United Kingdom*

ABSTRACT

According to Eurocode 8, the seismic design of flat-bottom circular silos containing grain-like material is based on a rough estimate of the inertial force imposed on the structure by the ensiled content during an earthquake: 80% of the mass of the content multiplied by the peak ground acceleration. A recent analytical consideration of the horizontal shear force mobilised within the ensiled material during an earthquake proposed by some of the authors has resulted in a radically reduced estimate of this load suggesting that in practice the *effective mass* of the contents is significantly less than that specified. This paper describes a series of laboratory tests that featured shaking table and a silo model which were conducted in order to obtain some experimental data to verify the proposed theoretical formulations and to compare with the established code provisions. Several tests have been performed with different heights of ensiled material – about 0.5 mm diameter Ballotini glass – and different magnitudes of grain-wall friction. The results indicate that in all cases the effective mass is indeed lower than the Eurocode specification, suggesting that the specification is overly conservative, and that the wall-grain friction coefficient strongly affects the overturning moment at the silo base. At peak ground accelerations up to around 0.35g, the proposed analytical formulation provides an improved estimate of the inertial force imposed on such structures by their contents.

Keywords: flat-bottom circular silos, grain-like material, seismic response, shaking-table tests, effective mass, friction coefficient.

1. INTRODUCTION

The structural design of flat-bottom circular silos containing grain-like material represents a challenging issue. The complex mechanism through whom the ensiled material interacts with the silo wall is under study from almost two centuries, many uncertainties still remain, and structural failures still occur. A brief overview about different silo failures and structural consequences during filling, discharging and strong ground motions can be found in literature [1, 2, 3, 4, 5].
The seismic assessment of such silos focuses on the estimation of the horizontal forces generated on the silo walls by the ensiled mass. In this respect, normal stresses and vertical and horizontal shear stresses are usually considered, and the seismic design of silos is usually performed on the basis of the identification of an *effective mass* which interacts with the silo walls under seismic excitation, i.e. the proportion of the total ensiled mass supported horizontally by the silo walls. The Eurocode 8 Part 4 [6] considers an effective mass equalling roughly 80% of the total ensiled mass, according to the research works by [2] and the analytical studies by[7, 8]. The effective mass is balanced by the

horizontal actions provided by the silo walls [6]. There is evidence that this formulation is too conservative [4, 9, 10]. By means of extensive numerical simulations, Holler and Meskouris [11] showed that, while the Eurocode 8 provisions provided a reasonable performance indicator for slender silos, squat silos should be associated with a reduction of the effective mass.
The concept of effective (or apparent) mass is also well established in the static design of silos (in particular, during filling) [12]. The Eurocode 1 Part 4 [13] refers to the approach proposed by Janssen [14, 15] and Koenen [16] for intermediate slender and slender silos and to the semi-empirical Reimbert's equation [17] for squat silos. However, an exhaustive background to conventional silo design can be found in [18, 3, 19, 20]. The static pressures during filling obtained by Janssen and Koenen were object of a large amount of experimental studies performed in the last two centuries, among which [21, 22, 23, 24, 25]. Other researchers focused on the experimental verification of the Janssen's theory in terms of apparent mass and confirmed the proposed formulation [26, 27, 28].
Differently from the research works behind the Eurocode 8 provisions, and starting from the widely verified approach adopted by Janssen [14, 15], Silvestri *et al.* [29] studied analytically the load imparted by an incompressible ensiled content, under constant horizontal acceleration, confined in a stiff cylindrical element [29]. While the analytical findings were obtained with reference to an idealised model (incompressible material and constant acceleration), they were consistent with the numerical results obtained by Holler and Meskouris [11] with reference to silo FEM models, and clearly confirmed that the Eurocode 8 provisions may lead to substantial overestimations of the seismic actions at the base of the silo.
In this framework, an exhaustive shaking-table experimental campaign has been carried out through a joint research work between the University of Bologna, the University of Alicante, the Polytechnic of Bari and the University of Bristol, in order to experimentally verify the proposed analytical formulation [29] and to gain preliminary insight on the issue of the effective mass acting on the silo walls in dynamic and seismic conditions.
This paper is organised as follows: first, it presents the results of this experimental campaign, in order to spread them to other researchers; second, it provides a comparison between the experimental results and the analytical predictions, in order to provide a new perspective on the dynamic behaviour of grain silos.
The final objective of this research (still under development) is to find out the important governing parameters for possible future implementation into structural design procedures and to propose hand-methods for a robust evaluation of the forces acting on the silo walls [5].

2. ANALYTICAL FRAMEWORK

Since the intention is to obtain experimental results to compare with analytical formulations, a brief summary of the analytical formulations is here presented.
In the research work by Silvestri *et al.* [29], an idealized system was considered to be representative of the ground-supported flat-bottom circular silo filled with grain-like material. The grain-like material was assumed to be incompressible and compact, as it were composed by a number of infinitely stiff and infinitely resistant spherical balls. In order to perform an integral evaluation of the global forces imparted by the grain to the silo walls, the grain was then treated as a set of overlapped layers of infinitesimal height dz', z' representing the distance of a single horizontal layer of grain from the top horizontal free surface. The silo walls could be assumed either infinitely stiff or flexible, with respect to the ensiled grain. This is relevant to the vertical profile of the horizontal acceleration along the height of the silo. The earthquake ground motion was simulated with time constant vertical and horizontal accelerations.
On the basis of dynamic equilibrium considerations, under the above-mentioned assumptions, and considering a uniform vertical profile of the horizontal acceleration along the height of the silo, the mutual actions exchanged between the grain and the silo walls were found:

$$p_{h,GW}(z,\theta)=\frac{\lambda\cdot\gamma\cdot z'}{\nu_0\left(1-\nu_0\cdot a_{eh0}\cdot\cos\theta\cdot\mu_{GW}\right)} \tag{1}$$

$$\tau_{v,GW}(z,\theta)=\mu_{GW}\cdot p_{h,GW}(z,\theta) \tag{2}$$

$$\tau_{h,GW}(z,\theta)=\left(\frac{a_{eh0}\cdot\sin\theta\cdot\gamma\cdot\lambda\cdot\mu_{GW}}{1-\nu_0\cdot a_{eh0}\cdot\cos\theta\cdot\mu_{GW}}\right)\cdot z \tag{3}$$

where $p_{h,GW}$ is the horizontal pressure exchanged between grain-wall; $\tau_{v,GW}$ and $\tau_{h,GW}$ are the vertical and horizontal shear stresses acting on the grain-wall interface, respectively; θ is the angle on the horizontal plane between the direction of the horizontal acceleration and the considered point in which the stresses are being evaluated; γ and λ are the specific weight and the pressure ratio of the grain-like material, respectively; a_{eh0} and a_{ev0} are the horizontal and vertical acceleration expressed as fractions of g, respectively; $\nu_0 = 1/(1+a_{ev0})$; μ_{GW} is the friction coefficient of the grain-wall contact surface.

Thus, according to [29], the following expressions represent the analytical shear force and the overturning moment at the base of the walls of the silo:

$$T=a_{eh0}\cdot\gamma\cdot\pi RH^2\left(\frac{\lambda\cdot\mu_{GW}}{\sqrt{1-\nu_0^{\,2}\cdot a_{eh0}^{\,2}\cdot\mu_{GW}^{\,2}}}\right) \tag{4}$$

$$M=\frac{1}{3}a_{eh0}\cdot\gamma\cdot\pi RH^3\left(\frac{\lambda\cdot\mu_{GW}}{\sqrt{1-\nu_0^{\,2}\cdot a_{eh0}^{\,2}\cdot\mu_{GW}^{\,2}}}\right) \tag{5}$$

where R is the radius of the circular silo and H is the height of the ensiled material.

The above analytical formulations have limits of validity which are related to the mathematical definition of some physical quantities. The following conditions are necessary:

$$\frac{H}{2R}<\frac{1-\nu_0\cdot a_{eh0}\cdot\mu_{GW}}{4\cdot\lambda\cdot\mu_{GW}} \tag{6}$$

$$a_{eh0}<\frac{1}{\nu_0\cdot\mu_{GW}} \tag{7}$$

$$a_{eh0}<\left(1-\frac{2\lambda\mu_{GW}H}{R}\right)\frac{1}{\nu_0\cdot\mu_{GW}} \tag{8}$$

$$a_{eh0}\le(1-|a_{ev0}|)\cdot\mu_{GB} \tag{9}$$

where μ_{GB} is the friction coefficient of the grain-base contact surface. These limitations are related to the mathematical definitions of some physical quantities: the first three arise from the existence conditions of the portions of grain leaning on the layers below and grain sustained by the walls, whilst the last one is related to the prevention of horizontal sliding of the grain core portion on the foundation. Additional details may be found in [29].

Conversely, Eurocode 8 provides two methods for obtaining the silo base shear force and overturning moment, herein referred to as “simplified” and “accurate”. Equations 10 and 11 represent the base shear and overturning moment provided by the simplified method:

$$T_{EC8,simplified}=a_{eh0}\cdot\gamma\cdot\pi\cdot R^2\cdot H\cdot 0.8 \tag{10}$$

$$M_{EC8,simplified}=a_{eh0}\cdot\gamma\cdot\pi\cdot R^2\cdot H\cdot 0.8\cdot\frac{H}{2} \tag{11}$$

Equations 12 and 13 represent the base shear and overturning moment provided by the accurate method:

$$T_{EC8,accurate} = a_{eh0} \cdot \gamma \cdot \pi \cdot R^2 \cdot H \left(1 - \frac{R}{6H}\right) \tag{12}$$

$$M_{EC8,accurate} = a_{eh0} \cdot \gamma \cdot \pi \cdot \frac{R^2}{2} \cdot \left(H^2 - \frac{R^2}{27}\right) \tag{13}$$

It is evident that, due to differences in models and basic assumptions, the pressure distributions and the wall base actions derived within this theory [29] differ from the Eurocode 8 provisions, which are basically grounded on the works by [2] and [7, 8]. In this paper, such differences will be investigated by means of a comparison between the analytical predictions, the Eurocode provisions and the experimental results of specifically developed shaking-table tests.

3. THE RATIONALE BEHIND THE EXPERIMENTAL CAMPAIGN

The objectives of the shaking-table tests are: (i) to experimentally verify the proposed analytical formulation [29]; ii) to get preliminary insight on the influence of the assumptions made on the base input (earthquake vs. constant acceleration).
Therefore, the experimental campaign has been designed both to meet the ideal conditions of the analytical theory and to investigate the influence of the type of input.
As far as objective 1 is concerned, the analytical theory [29] has been developed with reference to an idealised model (the grain-like material is uncompressible) in idealised conditions (the silo is subjected to a time constant acceleration). Since the theory is exquisitely analytical and thus independent from geometrical dimensions, any cylindrical element filled with uncompressible particulate material can be consistently used to represent the idealised model. Since the theory is developed for time constant acceleration, and given that shaking table cannot apply a time constant motion, low frequency sinusoidal inputs have been applied at the base of the cylinder. Using low frequency (namely, 1 and 2 Hz) sinusoidal input, it is possible to achieve a large duration for which the acceleration can be reasonably considered constant in time (around the peak of the sinusoid). The comparison between the analytical formulation and the experimental results has been performed basically in terms of overturning moment at the silo base.

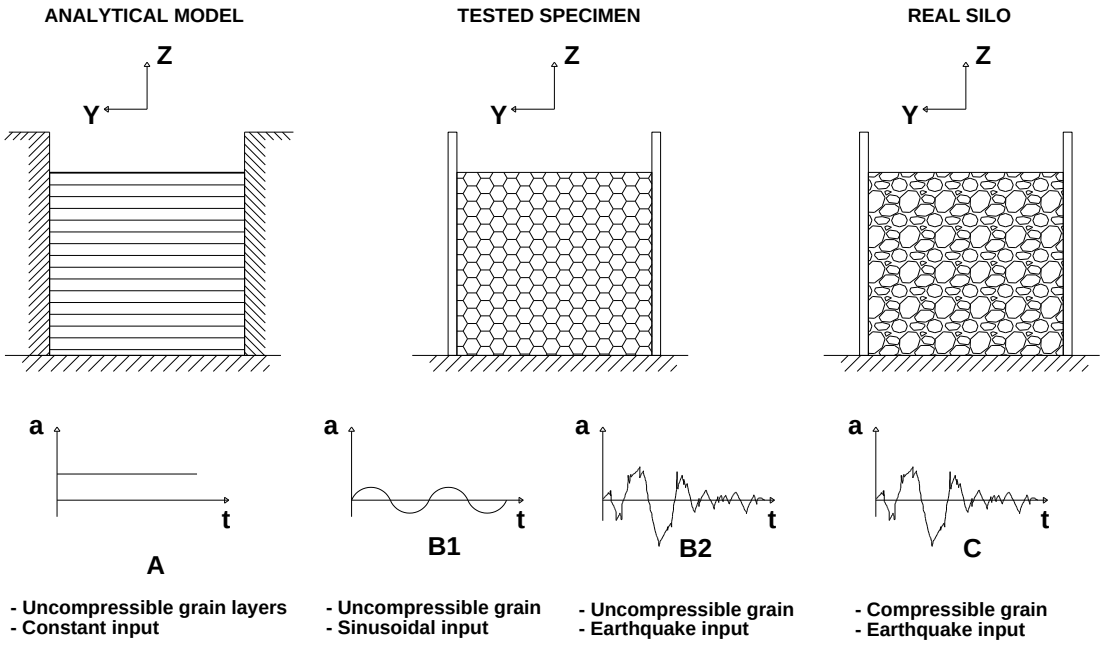

Figure 1. The analytical model, the tested specimen and the real silo.

As far as objective 2 is concerned, accelerograms of real earthquake ground motions have been utilised to investigate input motion dependence of response: in this respect, the vertical profile of the horizontal acceleration along the height of the silo has been monitored. The analytical theory [29] is capable of accounting for dynamic interaction between the ensiled grain and the silo walls, by means of general formulations which can be specified by introducing the actual (measured) vertical profile of the horizontal acceleration along the height of the silo.
It is worth pointing out that the use of the experimental evidences of these shaking-table tests to extrapolate information on the seismic behaviour of real silo structures is another issue, which is beyond the objectives of the present paper. In this regard, it is clear that, in the field, real flat-bottom silo systems are characterised by a compressible grain material and can be subjected to a broadband seismic acceleration. For sake of possible future transition from the idealised model of the theory to the "actual" case of real silos, Figure 1 provides the logical framework of the transition from the idealised conditions of the analytical model [29] to the tested specimen, and to the actual conditions of a real silo.

4. THE EXPERIMENTAL CAMPAIGN

4.1 The silo specimen

A circular silo specimen has been developed and realised to meet at best the idealised conditions, upon which the analytical formulation [29] to be verified is grounded. Given that the dimensions of the EQUALS shaking table are 3 m × 3 m, the specimen consists of a 1.2 m diameter, 1.5 m tall, 3 mm wall thickness polycarbonate container (Figure 2a). The circular silo was produced by bending two polycarbonate sheets to be semicircular in plan and fastening together the adjoining straight edges. Perspex rings encircle the tube at its top and bottom extremities so that it retains the intended shape. Polycarbonate ($E_{polycarbonate}$ = 2.3 GPa, $\nu_{polycarbonate}$ = 0.37) is selected due to the relatively low Young Modulus which has the effect of increasing the magnitude of mobilized strain thereby facilitating its measurement. The base of the container is covered with sandpaper to increase the grain-base friction coefficient, in order to meet the conditions related to the limits of validity of the theory (Eq. (9)). Both smooth and roughened (through application of sandpaper) walls are considered in the tests (Figures 2a and b).

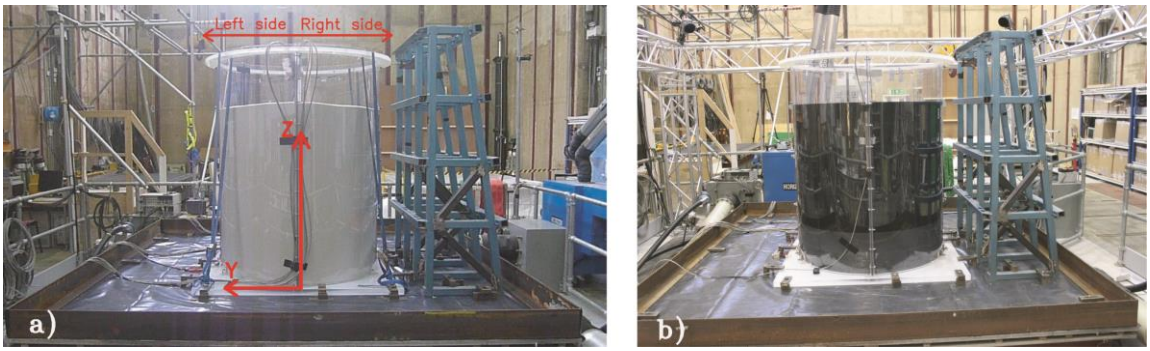

Figure 2. (a) The specimen with smooth walls. (b) The specimen with roughened walls.

4.2 The ensiled content

The silo specimen has been filled up to different heights (corresponding to different test configurations), H_i, with Ballotini glass material (Figures 3a and b) selected for both the regularity of the particles and their density when deposited (ρ = 1480 kg/m^3) leading to a total weight (20 kN) compatible with the payload capacity of the shaking table system (150 kN). A diameter of about 0.4-0.6 mm for the Ballotini glass beads has been selected.

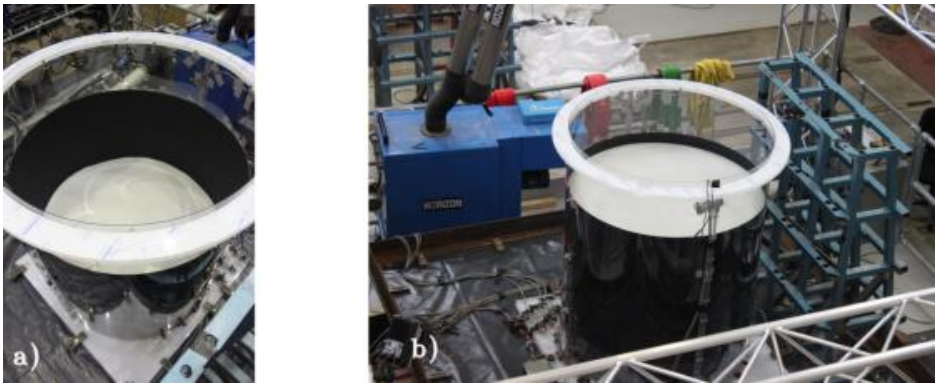

Figure 3. (a) The specimen filled with Ballotini glass up to 0.6 m. (b) The specimen filled with Ballotini glass up to 1.2 m.

The friction coefficients of the ensiled content (grain-grain, grain-wall and grain-base friction coefficients) have been evaluated using a modified direct shear apparatus [30]. Tests have been performed at appropriate densities and stress levels (5, 10, 15, 20 kPa) and this may introduce some uncertainties into results. The stress level is extremely low for available test equipment (only a few percentage of the apparatus capacity). Also, it was difficult to prepare samples of low density consistently.

For the grain-grain friction coefficient (μ_{GG}), i.e. the internal friction angle of the material (φ), Figure 4 provides the results of the shear-box tests, in terms of (a) the ratio between the shear stress (τ_{xy}) and the vertical normal stress (σ_z) as a function of the horizontal displacement (u_x), and (b) the dilatancy ($\frac{du_z}{du_x}$) as a function of the horizontal displacement (u_x). The peak direct shear angle of friction is derived from the maximum values assumed by the lines in Figure 4a, which are comprised in the range:

$$\mu_{GG} = tan\varphi = \frac{\tau_{xy}}{\sigma_x}\Big|_{max} \cong 0.45 \sim 0.50 \tag{14}$$

Reliable values for the internal friction angle are in the range of $\varphi = 24.2° \sim 26.6°$.

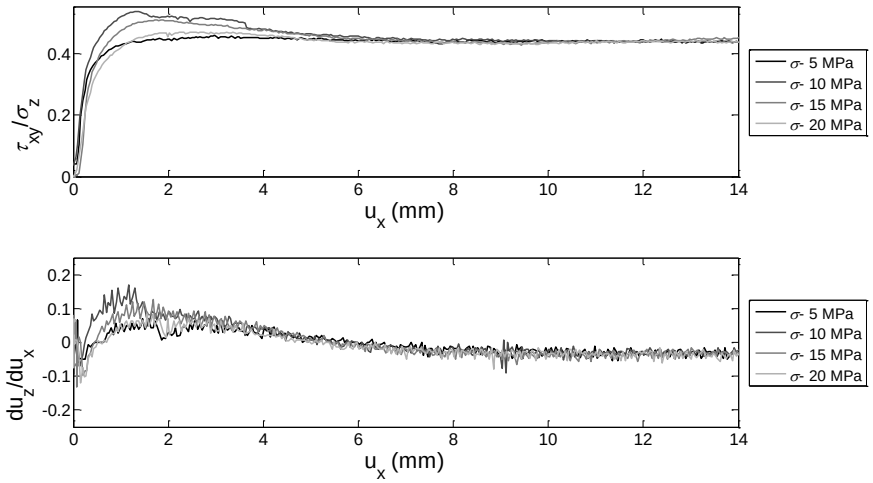

Figure 4. Shear-box test results.

For grain-wall (μ_{GW}) and grain-base (μ_{GB}) friction coefficients, Figure 5 provides the results of the interface tests, as conducted with the lower half of the apparatus replaced by either a polycarbonate sample (smooth interface) or a polycarbonate sample covered with sandpaper (rough interface), in

terms of (a) the ratio between the shear stress (τ_{xy}) and the vertical normal stress (σ_z) as a function of the horizontal displacement (u_x), and (b) the dilatancy ($\frac{du_z}{du_x}$) as a function of the horizontal displacement (u_x). The tangent of the stress ratio gives the angle of interface friction as:

$$\mu = \tan\varphi = \left.\frac{\tau_{xy}}{\sigma_z}\right|_{\max} \tag{15}$$

The evolution of τ_{xy}/σ_z with u_x is presented for the smooth and rough interface in Figures 5a and b, respectively, from which values of $\mu_{GW} = 0.30$ (Figure 5a) and $\mu_{GW} = 0.45$ (Figure 5b) can be derived. Given that the base of the silo has been covered with the same sandpaper used for the roughened walls, a grain-base friction coefficient equal to $\mu_{GB} = 0.45$ is applicable.

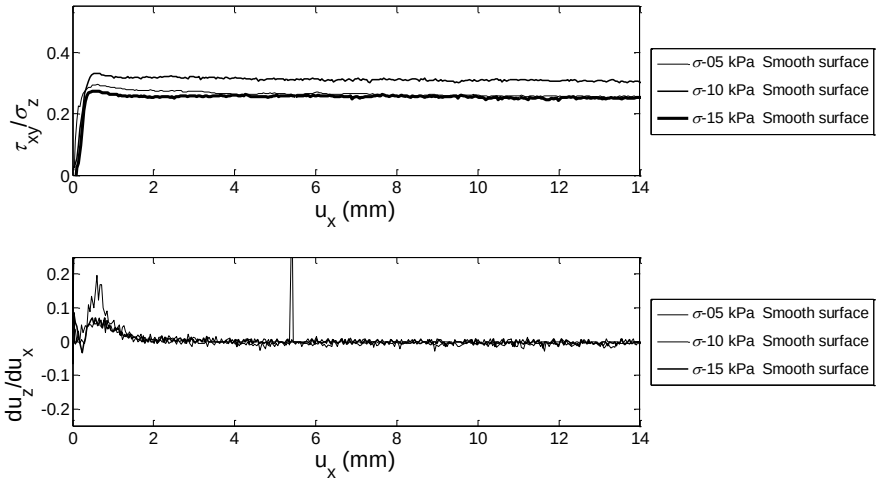

(a)

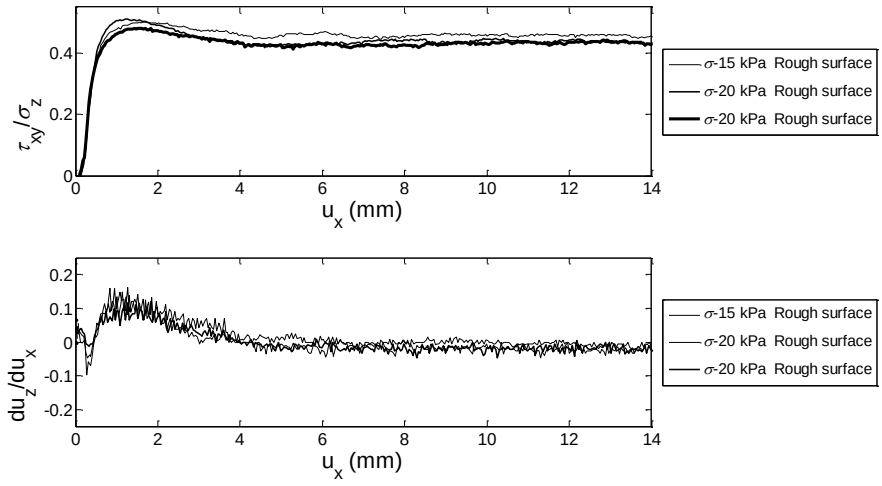

(b)

Figure 5. (a) Smooth interface tests results. (b) Rough interface tests results.

The Ballottini glass pressure ratio λ has not been directly measured. As clearly stated by [31, 32], neither theoretical formulations nor code provisions should be adopted for the evaluation of the pressure ratio via the angle of internal friction, especially for great value of φ. As a matter of fact,

the inferred values found by many researchers appear quite disperse [27, 28, 33, 34), since, in general, they result from back analyses developed to get the best matching between theoretical formulations and experimental data. Despite the common use of glass beads for experimental tests involving bulk material [34], no direct measurements are available in the technical and scientific literature, except from the aforementioned work by [31, 32]. In this work, for a glass beads bulk solid characterized by φ=27°, ρ=1726 kg/m^3, and diameter of about 1 mm, poured in an aluminum cylinder ($\mu_{GW} = 0.31$) for a 35kPa vertical stress level, the authors experimentally found a pressure ratio λ equal to 0.65 (to be used in the Janssen formulation).
Since the Ballottini glass features are similar to those of the glass beads tested by [31, 32] and since the grain-wall friction coefficient for the smooth wall configuration matches the one found by [31, 32], the same value of λ=0.65 has been here adopted in the interpretation of the results. From an engineering point of view, this value is consistent with the one obtained with the following relationship (holding for fully mobilised friction) [35, 36, 37]:

$$\lambda = \frac{1-sin^2\varphi}{1+sin^2\varphi} = 0.67 \sim 0.71 \quad (16)$$

4.3 Test configurations

By varying the grain-wall interface properties and the height of the ensiled content, three different configurations have been tested:

1. First, the silo characterised by smooth walls ($\mu_{GW} = 0.30$) and filled with Ballotini glass up to a height equal to H_1 = 1.2 m has been tested under white noises (N), sinusoidal inputs (S) and earthquake accelerograms (E), as applied along the Y horizontal direction.
2. Second, the silo characterised by roughened walls ($\mu_{GW} = 0.45$) and filled with Ballotini glass up to a height equal to H_2 = 0.60 m has been tested under white noises, sinusoidal inputs and earthquake accelerograms, as applied along the Y horizontal direction.
3. Third, the silo characterised by roughened walls ($\mu_{GW} = 0.45$) and filled with Ballotini glass up to a height equal to H_3 = 1.2 m has been tested under systematic sinusoidal inputs, as applied along the Y horizontal direction.

As illustrative example, Table 1 gives details about the test sequence performed for the first configuration. This list is here provided in order to better contextualize the selected results which will be described in next section 5 (especially, the ones concerning frequency changes, grain compaction, and accelerations).

Table 1. Test input for the first configuration of tests

INPUT	Tests No.	Table acceleration
White noise	N1 - N5	0.05 g – 0.30 g
1 HZ sinusoidal (Y)	S1 - S8	0.05 g – 0.40 g
White noise	N6	0.30 g
1 HZ sinusoidal (Y)	S9	0.03 g
0.5 HZ sinusoidal (Y)	S10 – S13	0.01 g – 0.15 g
White noise	N7	0.30 g
1 HZ sinusoidal (Y)	S14	0.50 g
White noise	N8	0.30 g

Earthquake input	E1- E18	0.04 g – 0.40 g
White noise	N9	0.30 g

4.4 Test setup

The test setup has been designed in order to provide measures of: (i) table, structure and grain accelerations at different locations, and (ii) structure deformations at different positions. The following instrumentation has been installed (Figure 6): (i) mono-directional accelerometers: some of them located at the shaking-table foundation, and some of them glued to the silo walls along two significant vertical generatrices; (ii) vertical and horizontal strain gauges positioned on the exterior side of the walls at four different heights along two significant generatrices, (iii) vertical strain gauges were added (at 45°) at the base circumference for the second and third test configurations (Figure 6b). The resulting base actions (due to the pressure distribution along the height of the silo) have been monitored by means of the strain gauges placed at the base of the silo walls.

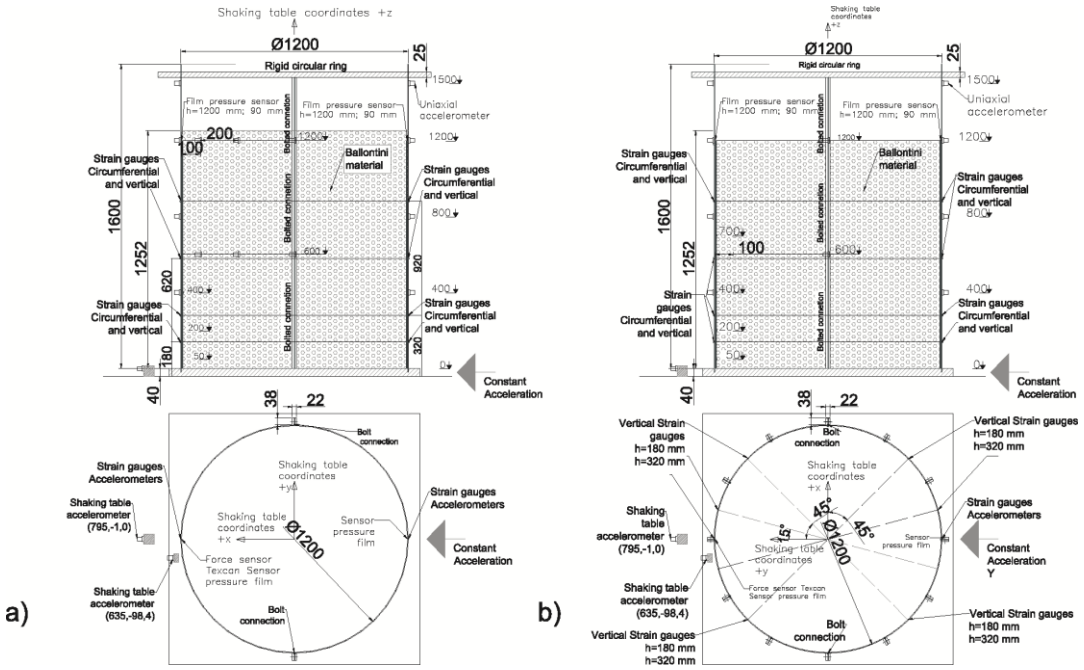

Figure 6. (a) The instrumentation in the first configuration. (b) The instrumentation in the second and third configuration.

5. RESULTS OF THE EXPERIMENTAL CAMPAIGN

5.1 Vertical settlements of the ensiled material

A progressive vertical settlement was observed during the tests, probably due to specimen compliance (circumferential cross-section deformation and local adjustments at the interlocking seam between the two U sections which constitute the specimen) and reorganization of the single glass beads with voids filling resulting in a global compaction. A 3-4 cm settlement (roughly 3% of the initial height) was measured in 13 positions, in terms of distance between a reference ideal line at the top silo level and the compacted free surface of the ensiled material (Figure 7), according to the same approach used by [38]. Figure 8 presents the content heights at the end of selected single tests with different 1 Hz sinusoidal inputs (see Table 1). The lines corresponding to the content free surface after each test indicate that a progressive settlement occurred. Under sinusoidal input, the ensiled material assumed a convex shape with maximum height in its central portion and minimum

height along the perimeter walls. On the other hand, strong earthquake input leaded to asymmetric distribution of the top layers.
From an engineering point of view, in the light of the negligible entity of the vertical settlements and of the incompressibility of the single glass beads, the assumption of uncompressible ensiled material is still reasonable.

Figure 7. Measurement of grain settlements.

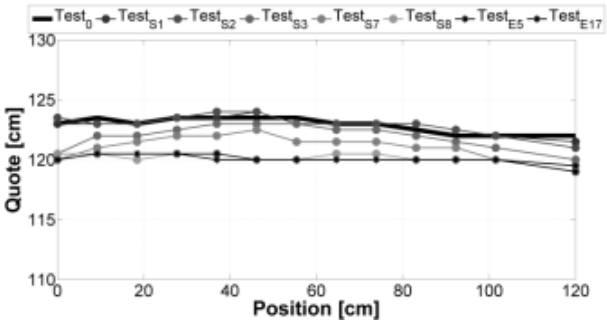

Figure 8. Grain heights at the end of selected single tests.

5.2 Frequencies

White noise inputs were used in order to evaluate the dynamic properties of the silo at increasing levels of peak base acceleration.
Figure 9 shows the transfer function of the silo-grain system as obtained with reference to the accelerometers placed on the shaking table and at the top of the silo (H = 1.5 m) for test N4. Two peaks are apparent, indicating that the dynamic behaviour of the silo-grain system is akin to a 2-degrees-of-freedom system. Also, the high values of the two frequencies suggest that a low-frequency sinusoidal input may effectively represent the constant input for the considered time ranges (around the peaks of the sinusoid), given that no dynamic interaction is expected between the input and the system frequencies. On the other hand, earthquake ground motion input characterised by frequencies comparable to the system frequency may lead to some dynamic interaction.
Table 2 presents the first two frequencies of the silo-grain system as obtained for the initial white noise tests in the first configuration. The first frequency reduces from 14.12 Hz to 12.72 Hz by increasing the peak base acceleration from 0.05 g to 0.30 g. This decrease in the frequency can be qualitatively explained by two phenomena: (i) the degradation of the "equivalent" shear modulus of the grain with increasing shear strains [39, 40] and (ii) the strong influence of grain-silo interaction in the dynamic response of these systems, which is deeply ruled by the grain-wall friction coefficient (the higher the friction, the higher the effective mass sustained by the walls) and by the type and magnitude of the exciting input (the higher the magnitude, the higher the effective mass), as also detected by [41].
The influence of test configuration on the fundamental system frequency as measured using 0.3g white noise excitation is shown in Table 3. It is apparent that the fundamental frequency increases with increasing wall friction and decreasing height of ensiled content.

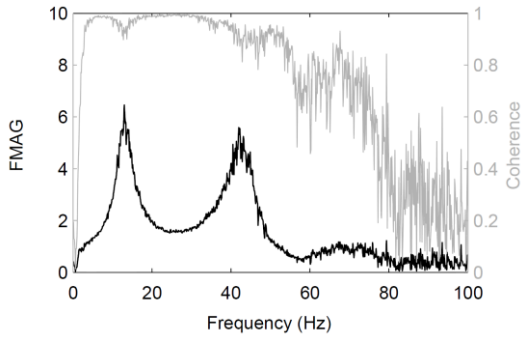

Figure 9. Transfer function of the silo-grain system for test N4.

Table 2. The first two frequencies identified in the white noise tests in the first configuration.

Test No.	Peak Base Acceleration Input	Frequency 1 [Hz]	Frequency 2 [Hz]
N2	0.05 g	14.1	44.9
N3	0.10 g	13.4	42.4
N4	0.20 g	12.9	42.8
N5	0.30 g	12.7	43.9

Table 3. Frequencies of the grain-silo system for each configuration.

Test configuration	Depth of ensiled material	Typology of silo walls	Fundamental frequency (Hz)
First	1.2 m	Smooth	12.7
Second	0.6 m	Rough	28.0
Third	1.2 m	Rough	16.0

5.3 Accelerations

Figure 10 shows the time-history of the horizontal acceleration at different heights of the silo for a 1Hz sinusoidal input with peak acceleration around 0.3g, for the left and right side of the silo (Figure 2a). The response recorded on the two sides of the silo is almost identical. The uniform response of the silo at different heights indicates negligible acceleration amplification thereby validating the assumption of uniform vertical profile of the horizontal acceleration along the height of the silo (physically related to the stiff behaviour of the silo-grain system).

Figure 11a represents the peak acceleration profiles (along the height of the silo walls) as obtained under different 1Hz sinusoidal inputs (see Table 1). These profiles are almost vertical (the variation of acceleration from the silo bottom up to height 0.84 m is less than 12%) for table accelerations lower than 0.35g: from an engineering point of view, negligible amplification occurs (no dynamic interaction). For the accelerometer placed on the top of the grain (height 1.24 m), the largest acceleration values which drift away from the vertical profile may be justified by the unavoidable horizontal sliding of the surface grain layers. On the other hand, amplifications up to 20% can be noted from the bottom to the top of the silo at accelerations above 0.35g. On the basis of these results, for table accelerations lower than 0.35g, the low-frequency sinusoidal input produces a near constant vertical profile of the horizontal acceleration.

Figure 11b represents the maximum acceleration at the top of the silo wall as a function of the table acceleration. A linear trend can be noted up to 0.35 g, where a slight slope change occurs. This is consistent with the limits of validity (Eq. (9)) of the theory which holds only for accelerations lower than $\mu_{GB} = 0.45$.

The second and the third configuration of tests present similar results for sinusoidal inputs. As illustrative examples, Figures 12a and b show the maximum acceleration at the top of the silo content as a function of the table acceleration for the second and the third configurations, respectively. A linear trend is obtained in both cases.
These figures are representative not only for the reported tests, but for all the 149 sinusoidal tests performed. The following conclusions can be achieved: the profile along the silo height of the horizontal acceleration under horizontal sinusoidal input is practically vertical. No acceleration amplification occurs for the silo-grain dynamic system under low-frequency sinusoidal input.

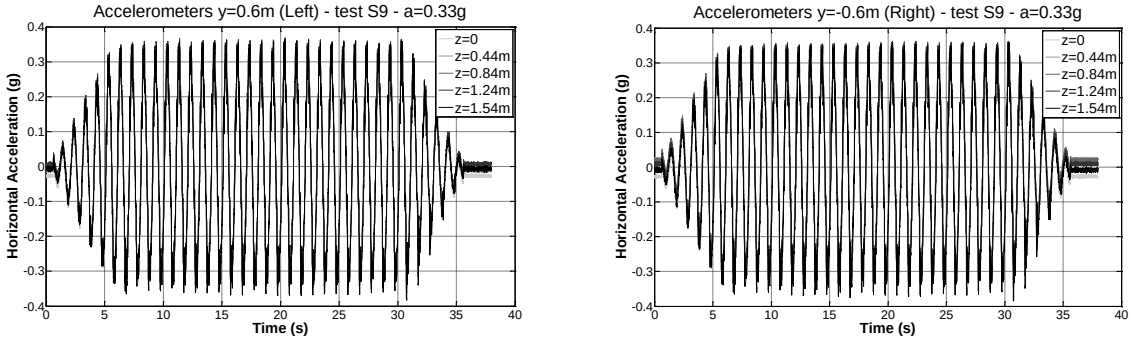

Figure 10. Accelerometers inside the silo at different heights (Left and Right in reference with Figure 2a) for the first configuration of tests.

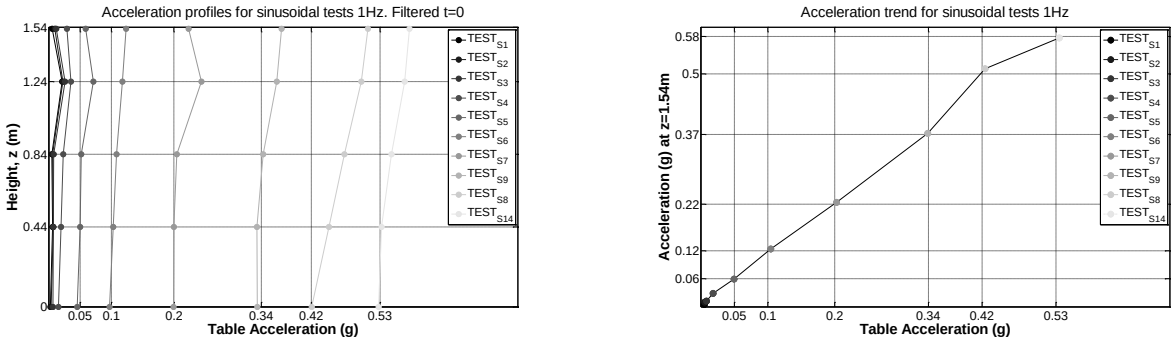

(a) (b)

Figure 11. (a) Acceleration profiles for sinusoidal tests at 1Hz. (b) Acceleration trend for sinusoidal tests at 1Hz.

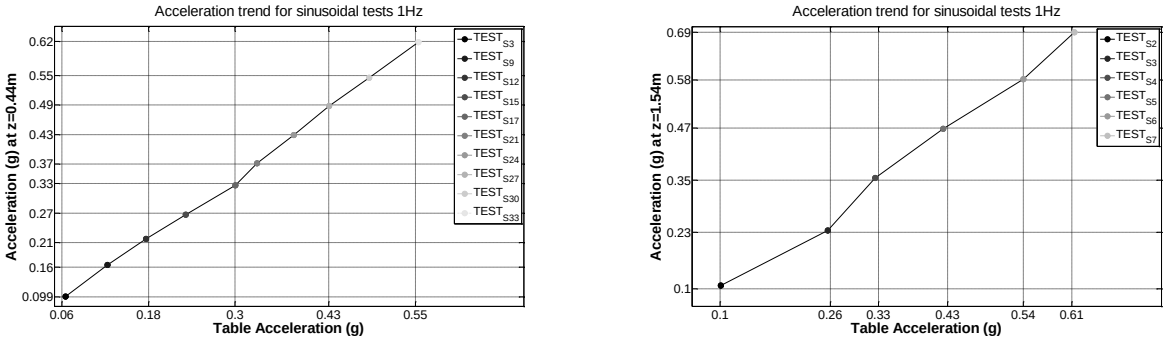

(a) (b)

Figure 12. (a) Acceleration profiles for sinusoidal tests second configuration. (b) Acceleration trend for sinusoidal tests third configuration.

5.4 Vertical strains

Figures 13a, b and c show the time-history of the vertical strains at different heights of the silo walls for a 1Hz sinusoidal input with peak acceleration around 0.3g, for the left side of the silo (Figure 2a) in the first, second and third configurations of test, respectively. In all cases, the response is sinusoidal like the input and symmetric with respect the initial strain level (herein set equal to zero). All strain gauges are in phase with increasing absolute values from the top to the bottom of the silo: the maximum vertical strain is reached at the lowest strain gauge (z = 0.18 m), whilst the minimum one is reached at the highest strain gauge (z = 0.92 m). This could be expected since the bending moment increases from the top to the bottom of the silo. It is interesting to note that the increase in the grain-wall friction coefficient (Figure 14c vs. Figure 14a) leads to higher strains at all heights, thus giving a first indication that the friction coefficient modifies the response of the system. Also, the reduction of the mass (Figure 13b vs. Figure 13c) obviously leads to lower strains.

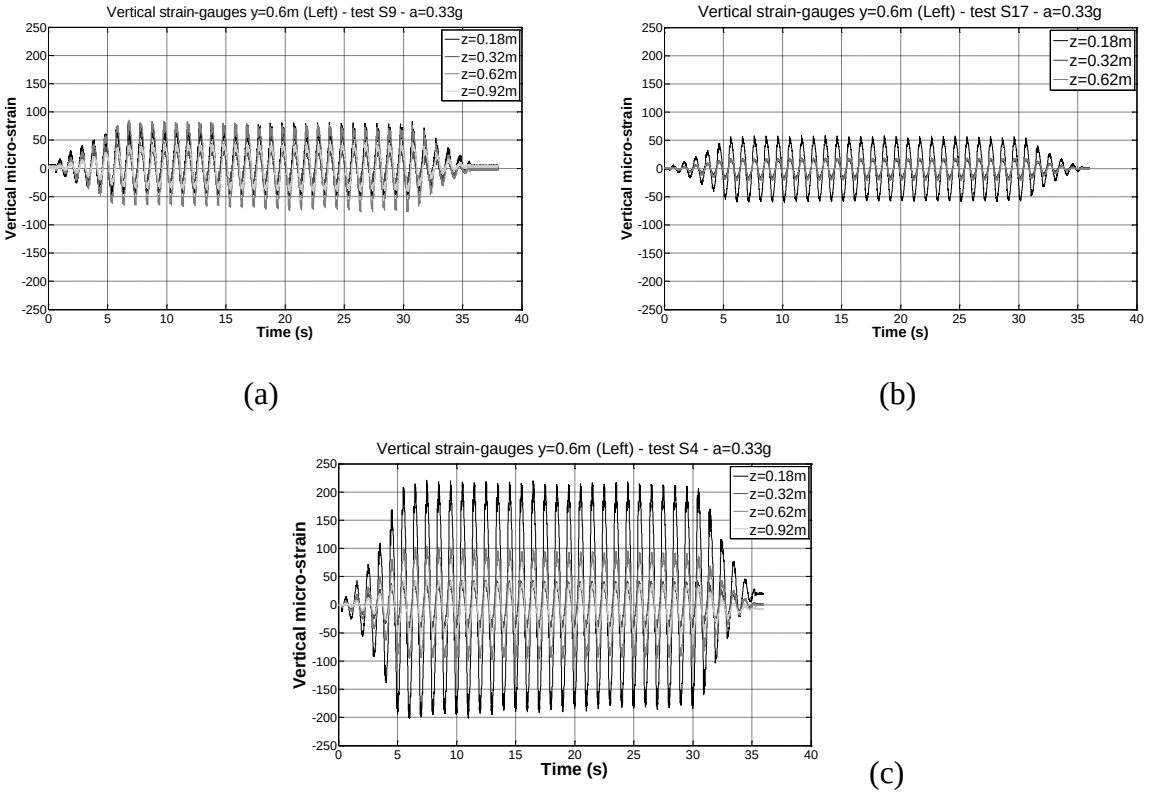

Figure 13. Vertical strains at different heights for the first (a), second (b) and third (c) configurations of tests.

As illustrative example, Figure 14 shows the mean of the vertical strains detected by the strain gauges symmetric with respect to the *y*-axis (placed according to Figure 17) and measured at the base (z=0.18 m), as a function of the y coordinate, for the 1Hz sinusoidal S4 input with peak acceleration around 0.3g (third configuration of tests) for three different time instants. The general trend appears rather asymmetric with respect to the *x*-axis. However, the vertical strains do not present a linear trend along the *y*-axis. This means that plane sections do not remain plane.
The order of magnitude of the highest vertical strains detected during the tests for the first, the second and the third configuration are around 550 $\mu\varepsilon$ (for 0.54 g), 180 $\mu\varepsilon$ (for 0.60 g) and 650 $\mu\varepsilon$ (for 0.60 g), respectively.

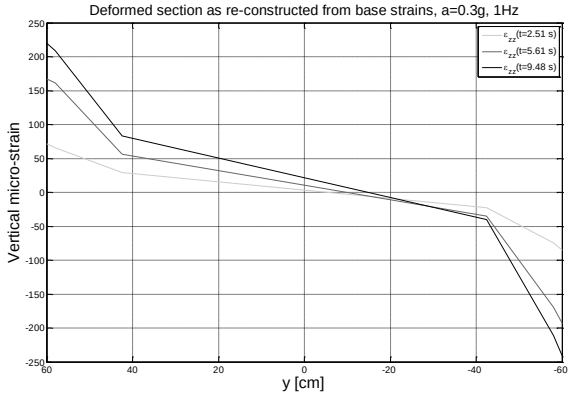

Figure 14. Vertical strains at z=0.14 m for the 1Hz sinusoidal S4 input.

5.5 Comparison between sinusoidal and earthquake response

To analyse the response of the silo specimen to a real earthquake where the excitation not only involves one frequency, several tests with different ground motion records are performed for each configuration. In order to excite the main frequencies of the silo-grain dynamic system, the South Iceland 2000 record has been selected for its particular spectral shape (Figure 15). This is characterised by high values at high frequencies (low periods), close to the main frequencies of the system.

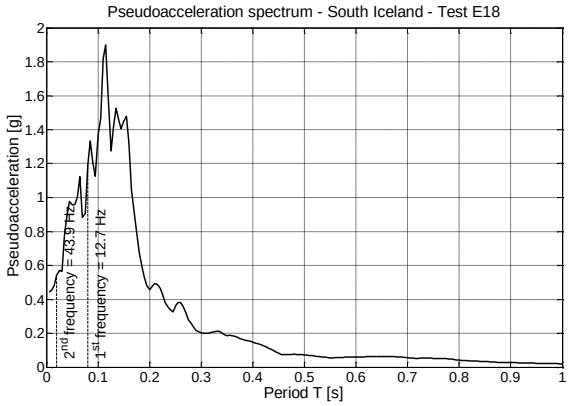

Figure 15. Pseudoacceleration spectrum of the table acceleration time-history for Test E18 (South Iceland earthquake) and fundamental frequencies of the silo-grain system.

Figure 16a shows the peak acceleration profiles along the silo height as obtained for different levels of the table acceleration, using the South Iceland earthquake as input, for the first test configuration. The profile is not linear, thus indicating an amplification of the base acceleration due to the frequency content of the selected input. In more detail, a bilinear trend can be recognised, with maximum amplification between 2 and 2.5 at the top of the silo. The response is thus substantially different from the case of sinusoidal input, for which no amplification occurs.
Figure 16b shows the peak acceleration at the top of the silo versus the peak table acceleration, using the South Iceland earthquake as input, for the first test configuration. The trend is linear up to 0.3g. Then a sudden change in the slope is obtained, which is consistent both with the limit given by Eq. (9) and with the results obtained for the case of sinusoidal input depicted in Figure 12b. In this case, the slope change is more marked due to the amplification effect.
On the basis of these results, the analytical theory can be applied to the case of earthquake input, if an appropriate (bilinear, in the case of the South Iceland earthquake) vertical profile is adopted for the horizontal acceleration.

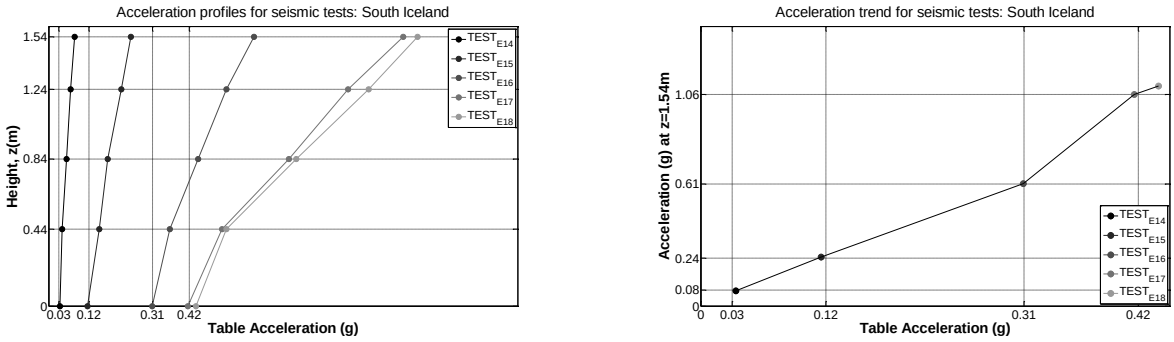

(a) (b)

Figure 16. (a) Acceleration profiles for seismic tests. (b) Acceleration trend for seismic tests.

6. INTERPRETATION OF THE RESULTS

6.1 The experimental base overturning moment

In order to reconstruct the experimental overturning moment at the base of the silo (z = 0.14 m), since the measurements indicate that plane sections do not remain plane (see previous section 5.4), a direct integration of the base vertical stresses multiplied by the corresponding lever arm over the whole circumferential cross-section has been performed.

In detail, the vertical strain, $\varepsilon_{zz,i}(t)$, as a function of time t, has been recorded for each i-th vertical strain gauge placed at z = 0.14 m: channels 3 and 15 for the first configuration (Figure 17) and channels 42, 2, 3, 4, 44, 43, 16, 15, 14 and 41 for the second and third configuration (Figure 17). Note that more precise results are obtained for the second and the third configuration of the tests, given that more strain gauges were placed at the base.

The corresponding vertical stress, $\sigma_{zz,i}(t)$, has been computed assuming linear elastic behaviour for the polycarbonate material of the silo:

$$\sigma_{zz,i}(t) = \frac{E_{polycarbonate}}{1-\left(\nu_{polycarbonate}\right)^2} \cdot \left(\varepsilon_{zz,i}(t) + \nu_{polycarbonate} \cdot \varepsilon_{\theta\theta,i}(t)\right) \tag{17}$$

where $\varepsilon_{\theta\theta,i}(t)$ is the circumferential strain recorded for each i-th horizontal strain gauge placed at z = 0.14 m. Then, the experimental overturning moment, $M_{\exp}(t)$, is obtained by direct integration of the base vertical stresses multiplied by their corresponding area, A_i, and lever arm, d_i, over the whole circumferential cross-section:

$$M_{\exp}(t) = \sum_i \sigma_{zz,i}(t) \cdot A_i \cdot d_i \tag{18}$$

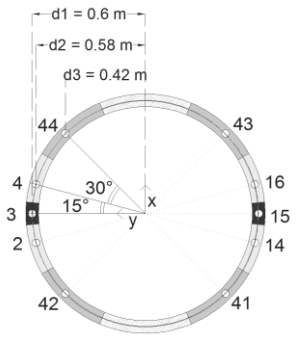

Figure 17. Plan view of the strain gauges position.

6.2 The influence of the wall-grain friction coefficient

The effect of the wall-grain friction coefficient is discussed in this section. Figure 18 compares the experimental base overturning moment as reconstructed from the base strain values, for the first (smooth walls) and the third (roughened walls) test configurations. In more detail, Figures 18a and b represent the moment derived from experimental measurements as a function of time, as obtained in the case of 1Hz sinusoidal input with peak table acceleration equal to 0.2g and 0.3g, respectively.

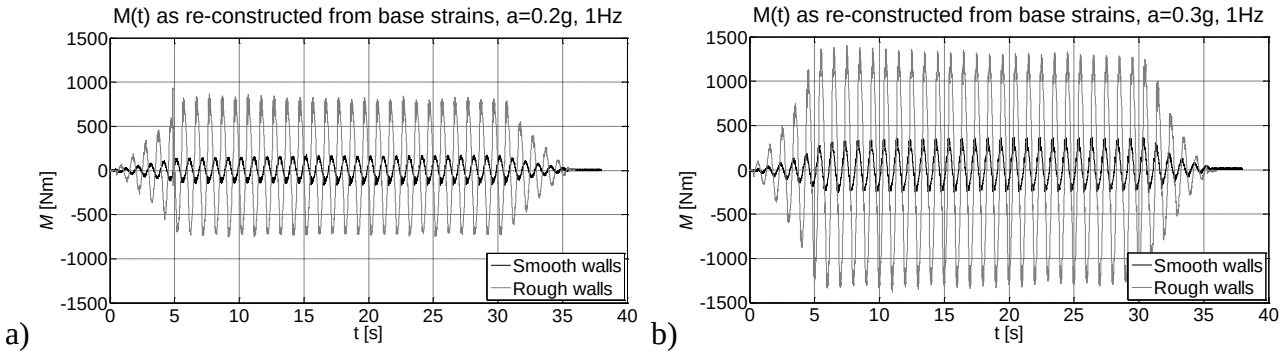

Figure 18. Comparison between the first and the third configuration overturning moments at (a) 0.2g and (b) 0.3g.

The results clearly indicate that the response of the silo with smooth walls is far less than the response of the silo with roughened walls. Thus, the wall-grain friction coefficient strongly affects the experimental base overturning moment.

Figure 19 represents the reconstructed value of the base overturning moment (the mean value over the maximum values obtained for each one of the 10-15 cycles of the sinusoidal input) as a function of the actual measured acceleration of the shaking-table, for all the three tests configurations. When comparing the first with the third configuration, a significant increment of the base moment is observed due to the increase of the grain-wall friction coefficient. When comparing the third with second configuration, an obvious decrement of the base moment is observed due to the reduction of the grain mass.

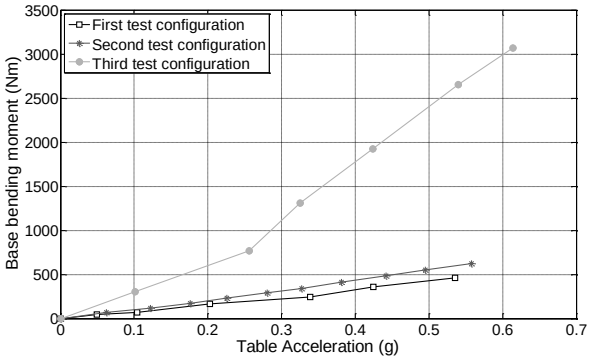

Figure 19. Base overturning moment vs. table acceleration for all the three test configurations.

The following conclusion can be drawn. The experimental results do not match with Eurocode 8 prescriptions which do not take into account the wall-grain friction coefficient at all. From a qualitative point of view, according to the analytical theory suggested by some of the authors [29], higher wall-grain friction coefficient (roughened walls) leads to higher actions inside the walls. This is a fundamental result.

In order to better show the effectiveness of the analytical theory in capturing the experimental results, a further comparison of the experimental base overturning moment between the first and the

third configuration (characterised by the same height of the silo content and different grain-wall friction coefficients) has been carried out from another point of view. The ratios between the experimental moment and the experimental moment corresponding to a selected horizontal acceleration ($\bar{a}_{eh0}$) are evaluated for both configurations:

$$\left.\frac{M_{\exp}(a_{eh0})}{M_{\exp}(\bar{a}_{eh0} \cong 0.55)}\right|_{\mu_{GW}=0.30} \quad \text{(first configuration)} \tag{19}$$

$$\left.\frac{M_{\exp}(a_{eh0})}{M_{\exp}(\bar{a}_{eh0} \cong 0.55)}\right|_{\mu_{GW}=0.45} \quad \text{(third configuration)} \tag{20}$$

and reported in Figure 20 as functions of the table acceleration. $\bar{a}_{eh0}$ has been chosen roughly equal to 0.55 g, since it is the maximum value reached in the first test configuration, thereby leading to a common domain for both configurations and allowing a consistent comparison.
Despite two different grain-wall friction coefficients, the two plots show the same bilinear trend, with slope change exhibited for the same value of the table acceleration (0.33 g) in both cases. This result can be analytically expressed by the following equality between the adimensional base overturning moments:

$$\left.\frac{M_{\exp}(a_{eh0})}{M_{\exp}(\bar{a}_{eh0} \cong 0.55)}\right|_{\mu_{GW}=0.30} \cong \left.\frac{M_{\exp}(a_{eh0})}{M_{\exp}(\bar{a}_{eh0} \cong 0.55)}\right|_{\mu_{GW}=0.45} \tag{21}$$

This is also confirmed by the theoretical counterpart of the experimental adimensional base overturning moment as evaluated using Eq. (5):

$$\frac{M(a_{eh0})}{M(\bar{a}_{eh0})} = \frac{a_{eh0}}{\bar{a}_{eh0}} \cdot \frac{\sqrt{1-\nu_0^{\,2} \cdot \bar{a}_{eh0}^{\,2} \cdot \mu_{GW}^{\,2}}}{\sqrt{1-\nu_0^{\,2} \cdot a_{eh0}^{\,2} \cdot \mu_{GW}^{\,2}}} \tag{22}$$

In fact, for values of a_{eh0}, $\bar{a}_{eh0}$ and μ_{GW} lower than unity, Eq. (28) can be approximated by:

$$\frac{M(a_{eh0})}{M(\bar{a}_{eh0})} \cong \frac{a_{eh0}}{\bar{a}_{eh0}} \tag{23}$$

which indicates that the theoretical adimensional base overturning moment (i) does not depend on the physical parameters of the system (among which the grain-wall friction coefficient), and (ii) increases linearly with the horizontal acceleration.

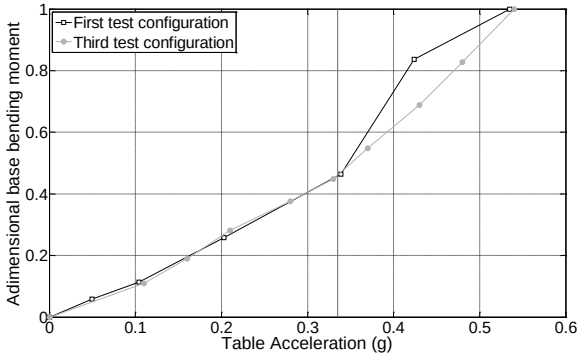

Figure 20. Adimensional base overturning moment vs. table acceleration for the first and the third test configurations.

6.3 The comparison between the experimental and the predicted values of the base overturning moment

In this section, the reconstructed base overturning moment is compared with the provisions of Eurocode 8 (simplified and accurate method) and the prediction of [29] (as evaluated considering a uniform vertical profile of the horizontal acceleration along the height of the silo, in accordance with the results of section 5.3) for both sinusoidal and earthquake inputs. Figures 21, 22 and 23 report this comparison for the case of sinusoidal input, for all three test configurations, respectively.
With reference to the the first configuration (full grain mass), the values obtained by the analytical theory represent a reasonable upper bound for the values of the experimental base overturning moment. With reference to the the third configuration (full grain mass), the values obtained by the analytical theory are in good agreement with the experimental results. With reference to the second configuration (half grain mass), the values obtained by the analytical theory are lower than the experimental results. A possible reason may lie in the disturbing effect of the mass of top ring, instrumentation and cables on the dynamic system behaviour, which becomes not negligible with respect to the half amount of grain. The analytical theory does not take into account the additional bending moments due these masses and the consequent alterations in the dynamic response.
With reference to all configurations, at different input frequencies and accelerations, the values of the experimental overturning moment at the base of the silo are far lower than the values obtained using the Eurocode 8 provisions. Thus it clearly seems that these provisions are overly conservative.
To analyze the silo response to real earthquake ground motion, Figure 24 represents the values of the experimental overturning moment at the base of the silo for three different earthquakes, together with the predicted values for the first configuration. Again, the analytical theory represents a reasonable upper bound for all values of the experimental base overturning moment. It is worth noticing that this is true also for the South Iceland earthquake (whose spectrum is reported in Figure 15) which represents the most demanding input for the considered system.

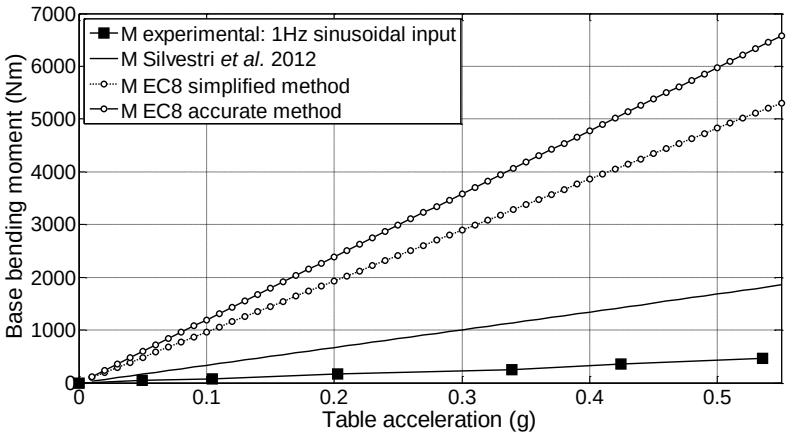

Figure 21. Comparison between the experimental overturning moment as obtained in the first test configuration for the 1 Hz sinusoidal input and the predicted values by the theory by Silvestri et al. 2012 and by the Eurocode 8 methods.

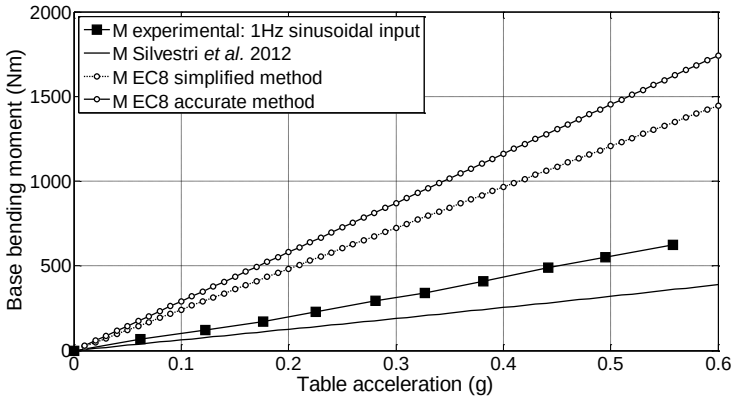

Figure 22. Comparison between the experimental overturning moment as obtained in the second test configuration for the 1 Hz sinusoidal input and the predicted values by the theory by Silvestri et al. 2012 and by the Eurocode 8 methods.

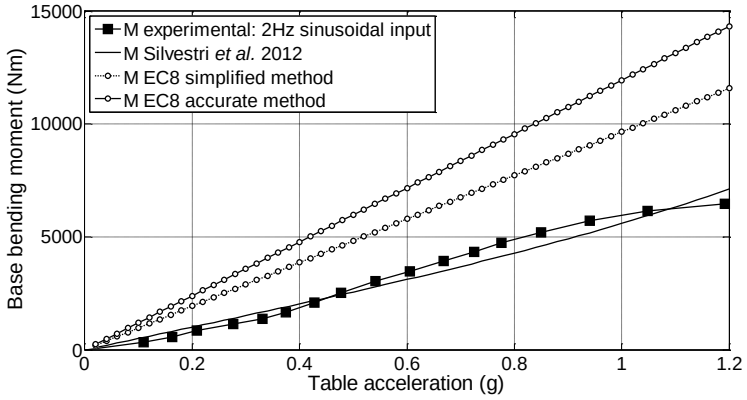

Figure 23. Comparison between the experimental overturning moment as obtained in the third test configuration for the 2 Hz sinusoidal input and the predicted values by the theory by Silvestri et al. 2012 and by the Eurocode 8 methods.

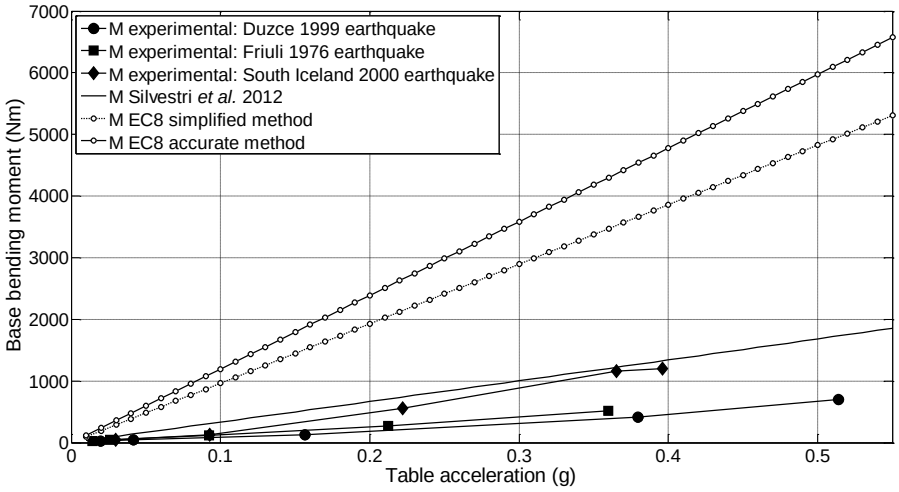

Figure 24. Comparison between the experimental overturning moment as obtained in the first test configuration for the three earthquakes: Duzce, Friuli, South Iceland and the predicted values by the theory by Silvestri et al. 2012 and by the Eurocode 8 methods.

7. CONCLUSIONS

This paper offers an experimental verification (via shaking table modelling) of an analytical model [29] regarding the actions induced by grain-like material upon the walls of flat-bottom silos.
In more detail, the objective of the shaking-table tests was to investigate the effects of the pressures exerted by the grain on the silo walls, in order to compare them with the Eurocode 8 provisions and with the analytical formulation, which was developed with reference to an idealised model (the grain-like material is uncompressible) in idealised conditions (the silo is subjected to a time constant acceleration). Low frequency sinusoidal input has been applied to meet at best the time constant acceleration assumption of the theory. Also, earthquake inputs have been used to further investigate the seismic response.
The following concluding remarks containing preliminary but yet clear indications can be drawn from the experimental campaign:

1. The vertical profile of the horizontal acceleration under low frequency sinusoidal input is almost constant, so that no acceleration amplification has to be considered for the silo-grain system.
2. The vertical profile of the horizontal acceleration under earthquake input is not linear, thus indicating a dynamic component in the system response.
3. The experimental results clearly indicate that the wall-grain friction coefficient strongly affects the experimental base overturning moment. This does not match with Eurocode 8 prescriptions which disregards the wall-grain friction coefficient. From a qualitative point of view, according to the analytical theory, higher wall-grain friction coefficient leads to higher actions inside the walls.
4. The values of the experimental overturning moment at the base of the silo are far lower than the values obtained using the Eurocode 8 provisions, for both sinusoidal and earthquake input. Thus, it clearly seems that these provisions are overly conservative.
5. On the other hand, the predicted values by the analytical theory are in good agreement (either reasonable upper bound or good approximation) with the experimental results.

ACKNOWLEDGEMENTS

The authors acknowledge the financial support received from the European Community's Seventh Framework Program [FP7/2007-2013] under grant agreement n° 227887 for the SERIES Project (ASESGRAM project: “Assessment of the seismic behaviour of flat-bottom silos containing grain-like materials”).
The authors would like to thank Francesco Fabbri, Giulia Lavatura and Erica Carboni for their contributions in the preliminary design of the experimental shaking table tests, together with Luca Pieraccini for his contributions in the interpretation of the results and in the final revision of the paper.

REFERENCES

1. Ravenet J (1981). Silo problems. Bulk Solids Handing, 1(4), 667-679.
2. Rotter JM, Hull TS (1989). Wall loads in squat steel silos during earthquakes. Engineering Structures, 11(3), 139-147.
3. Nielsen J (1998). Pressures from flowing granular solids in silos. Philosophical Transactions-Royal Society of London Series A Mathematical Physical and Engineering Sciences, 2667-2684.
4. Dogangun A, Karaca Z, Durmus A, Sezen H (2009) Cause of Damage and Failures in Silo Structures, Journal of Performance of Constructed Facilities ASCE, Vol. March-April, 65-71.
5. Knoedel P (2008). Recent silo codes–and still structural failure?. Structures and Granular Solids: From Scientific Principles to Engineering Application, 113.

6. EN 1998-4 (2006) Eurocode 8. Design of structures for earthquake resistance, Part 4 -Silos, tanks and pipelines, CEN, Brussels.
7. Younan AH, Veletsos AS. (1998). Dynamics of Solid-Containing Tanks. I: Rigid Tanks. Journal of Structural Engineering, 124(1), 52-61.
8. Veletsos A., Younan AH. (1998). Dynamics of solid-containing tanks. II: Flexible tanks. Journal of Structural Engineering, 124(1), 62-70.
9. Dvornik J, Lazarevic D (1999). Loading of granular material on silo walls. In : Processing of the 1st conference on applied mathematics and computation, Dubrovnik, Croatia, 13-18 Sept 1999, pp 215-222.
10. Wagner R, Noh S-Y, Butenweg C, Meskouris K (2002). Seismic excited granular material silo. In Grundmann H, Schueller GI (eds) Proceedings of Eurodyn 2002, pp 253-258. ISBN:90 5809510X:307-333
11. Holler S, Meskouris K (2006). Granular material silos under dynamic excitation: numerical simulation and experimental validation. J Struct Eng ASCE 132(10):1573-1579.
12. Pozzati P, Ceccoli C (1972) Teoria e Tecnica delle Strutture, Volume Primo, Preliminari e Fondamenti. UTET, Torino.
13. EN 1991-4 (2004) Eurocode 1. Basis of design and action on structures. Part 4. Actions in silos and tanks. CEN, Brussels.
14. Janssen HA (1895) Versuche uber Getreidedruck in Silozellen. Zeitschrift des vereines deutcher Ingenieure, August 1895, p. 1045.
15. Sperl M (2006). Experiments on corn pressure in silo cells–translation and comment of Janssen's paper from 1895. Granular Matter, 8(2), 59-65.
16. Koenen M (1896) Berechnung des Seiten und Bodendrucks in Silozellen, Centralblatt der Bauverwaltung, Vol. 16, p. 446-449.
17. Reimbert ML, Reimbert AM (1976). Silos: theory and practice (p. 251). Trans Tech Publications.
18. Safarian SS, Harris EC (1985). Design and construction of silos and bunkers. New York: Van Nostrand Reinhold.
19. Brown CJ, Nielsen J (Eds.). (1998). Silos: fundamentals of theory, behaviour and design. CRC Press.
20. Rotter JM (2001). Guide for the economic design of circular metal silos. New York: Spon Press
21. Jamieson JA (1903). Grain pressures in deep bins. CSCE Transactions 17:554-607.
22. Amundson LR (1945). Determination of band stresses and lateral wheat pressures for a cylindrical grain bin. Agricultural Engineering, 26, 321-345.
23. Negi SC, Ogilvie JR, Norris ER, (1977). SILAGE PRESSURES IN TOWER SILOS. PART 3. EXPERIMENTAL MODEL STUDIES AND COMPARISON WITH. CANADIAN AGRICULTURAL ENGINEERING, 19(2).
24. Schwab CV, Ross IJ, White GM, Colliver DG, (1994). Wheat Loads and Vertical Pressure Distribution in a Full-scale Bin Part I—Filling. Transactions of the ASAE, 37(5), 1613.
25. Tatko R, Kobielak S (2008) Horizontal bulk material pressure in silo subjected to impulsive load. Shock and Vibration, vol. 15, p. 543-550.
26. Vanel L, Clément E, (1999). Pressure screening and fluctuations at the bottom of a granular column. The European Physical Journal B-Condensed Matter and Complex Systems, 11(3), 525-533.

27. Vanel L, Claudin P, Bouchaud JP, Cates ME, Clément E, Wittmer JP, (2000). Stresses in silos: comparison between theoretical models and new experiments. Physical review letters, 84(7), 1439.
28. Ovarlez G, Fond C, Clément E, (2003). Overshoot effect in the Janssen granular column: a crucial test for granular mechanics. Physical Review E, 67(6), 060302.
29. Silvestri S, Gasparini G, Trombetti T, Foti D (2012) On the evaluation of the horizontal forces produced by grain-like material inside silos during earthquakes. Bulletin of Earthquake Engineering, vol. 10, p. 1535-1560.
30. Lings ML, Dietz MS (2004) An improved direct shear apparatus for sand, Géotechnique, Volume 54, Issue 4, pages 245 –256
31. Kwade A, Schulze D, Schwedes J, 1994a. Determination of the stress ratio in uniaxial compression tests-Part 1. Powder Handling and Processing, 6(1), 61-65.
32. Kwade A, Schulze D, Schwedes J. (1994). Determination of the stress ratio in uniaxial compression tests-Part 2. Powder Handling & Processing, 6(2), 199-203.
33. Arroyo-Cetto D, Pulos G, Zenit R, Jimenez-Zapata MA, Wassgren CR, (2003). Compaction force in a confined granular column. Physical Review E, 68(5), 051301.
34. Mandato S, Cuq B, Ruiz T, (2012). Experimental study of vertical stress profiles of a confined granular bed under static and dynamic conditions. The European Physical Journal E: Soft Matter and Biological Physics, 35(7), 1-8.
35. Krynine DP, (1945). Discussion of "Stability and stiffness of cellular cofferdams" by Karl Terzaghi. Transactions, ASCE, 110, 1175-1178.
36. Dabrowski A, (1957). Parcie Materialow Sypkich w Leju (Pressures from bulk solids in hoppers). Archiwum Inzynierii Ladowej, Warsawa, 325-328.
37. Buisman ASK, (1940). Grondmechanika, Waltman.
38. Ueng TS, Wu CW, Cheng HW, Chen CH (2010) Settlements of saturated clean sand deposits in shaking table tests. Soil Dynamics and Earthquake Engineering, vol. 30, p. 50-60.
39. Seed HB, Idriss IM (1970) Soil moduli and damping factors for dynamic response analyses. Report EERC 70-10, Earthqauke Engineering Research Center, University of California, Berkeley.
40. Kramer S.L. (1996) Geotechnical Earthquake Engineering, Prentice Hall Inc., Upper Saddle River, NJ 07458.
41. Yokota H, Sugita M, Mita I, (1983, November). Vibration tests and analyses of coal-silo model. In Proc., 2nd Int. Conf. on the Design of Silos for Strength and Flow, Stratford-upon-Avon, Powder Advisory Centre (November 1983) (pp. 107-116).